Synthesis of surfactant-free electrostatically stabilized gold nanoparticles by plasma-induced liquid chemistry

2013 Nanotechnology 24 245604

(http://iopscience.iop.org/0957-4484/24/24/245604)

Nanotechnology **24** (2013) 245604 (11pp) doi:10.1088/0957-4484/24/24/245604

Synthesis of surfactant-free electrostatically stabilized gold nanoparticles by plasma-induced liquid chemistry

J Patel[1], L Němcová[2,3], P Maguire[1], W G Graham[2] and D Mariotti[1]

[1] Nanotechnology and Integrated Bio-Engineering Centre (NIBEC), University of Ulster, Newtownabbey BT37 0QB, UK
[2] Centre for Plasma Physics, School of Mathematics and Physics, Queen's University Belfast, University Road, Belfast BT7 1NN, UK
[3] Brno University of Technology, Faculty of Chemistry, Purkynova 118, Brno 61200, Czech Republic

E-mail: patel-j1@email.ulster.ac.uk

Received 3 January 2013, in final form 2 April 2013
Published 21 May 2013
Online at stacks.iop.org/Nano/24/245604

Abstract
Plasma-induced non-equilibrium liquid chemistry is used to synthesize gold nanoparticles (AuNPs) without using any reducing or capping agents. The morphology and optical properties of the synthesized AuNPs are characterized by transmission electron microscopy (TEM) and ultraviolet–visible spectroscopy. Plasma processing parameters affect the particle shape and size and the rate of the AuNP synthesis process. Particles of different shapes (e.g. spherical, triangular, hexagonal, pentagonal, etc) are synthesized in aqueous solutions. In particular, the size of the AuNPs can be tuned from 5 nm to several hundred nanometres by varying the initial gold precursor ($HAuCl_4$) concentration from 2.5 μM to 1 mM. In order to reveal details of the basic plasma–liquid interactions that lead to AuNP synthesis, we have measured the solution pH, conductivity and hydrogen peroxide (H_2O_2) concentration of the liquid after plasma processing, and conclude that H_2O_2 plays the role of the reducing agent which converts Au^{+3} ions to Au^0 atoms, leading to nucleation growth of the AuNPs.

S Online supplementary data available from stacks.iop.org/Nano/24/245604/mmedia

(Some figures may appear in colour only in the online journal)

1. Introduction

In recent years there has been a tremendous growing interest in the field of gold nanoparticles (AuNPs) and their applications [1–4] with a range of synthesis methods for metal NPs that are being investigated or that are currently in use (e.g. chemical synthesis by using reducing and capping agent [5], biosynthesis [6], laser ablation method [7] etc). More recently, stable generation of plasmas at atmospheric pressure [8–12] has given the opportunity to explore a new range of approaches for nanomaterials synthesis and various configurations have been reported to synthesize AuNPs directly in liquids (e.g. plasma generated by electrodes immersed in liquids [13–16], gas–liquid interfacial low-pressure plasmas [17], atmospheric pressure plasma interfacing with liquid [8, 18–20] etc). Because of unique characteristics, microscale plasmas (i.e. microplasmas) offer specific advantages for nanomaterials synthesis [8, 12, 21, 22] and for interacting with liquids [8, 23–34] so that microplasma-induced synthesis and surface engineering of nanomaterials directly in liquids have been recently investigated [2, 23, 35]. Microplasma–liquid interactions have therefore initiated new synthetic and functionalization approaches that are different from both standard liquid electrochemistry as well as from

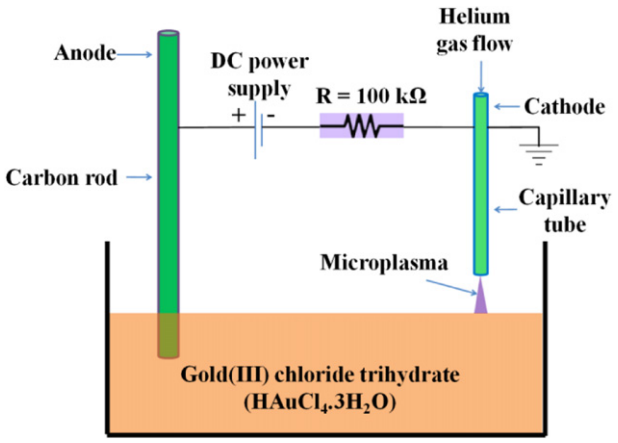

Figure 1. Atmospheric pressure microplasma setup used for the synthesis of gold nanoparticles.

gas-phase plasma synthesis. These new approaches based on plasma-induced non-equilibrium liquid chemistry have a great potential of combining some of the best advantages of plasma processing (e.g. non-equilibrium kinetics) and wet chemistry (e.g. solution processing) [36].

Current synthesis approaches, however, still present limitations that relate to the quality of the synthesized materials in terms of size and shape, process cost and complexity, safety, production rate, throughput etc [8, 19]. For instance, most of these methods, including plasma–liquid systems, have required so far reducing and/or capping agents to synthesize/stabilize the AuNPs and therefore additional processing steps are needed to eliminate undesired chemicals from the surface of AuNPs or from the solution. Furthermore, while the work carried out on plasma–liquid interactions have shown the possibility of tuning morphology and size, an in-depth study on the processing parameters leading to a better understanding of the fundamental synthesis mechanisms is still missing.

In the present study, we have used a simple-to-use, one-step, few-minute approach based on an atmospheric pressure microplasma which directly interacts with liquids to synthesize colloidal and electrostatically stabilized AuNPs. This synthesis technique does not need any added reducing and/or capping agents and only requires a water-based solution with the metal precursor. More specifically, in this study, the effects of gold precursor concentration and of the discharge current on the particle formation process are analysed. AuNPs are synthesized by processing aqueous solutions with $HAuCl_4$ precursor at different molar concentrations by microplasma with different discharge currents. Ultraviolet–visible (UV–vis) spectroscopy, transmission electron microscopy (TEM) and zeta sizer instrument are used to characterize the synthesized AuNPs. We also provide a description of the fundamental mechanisms and reaction paths that contribute to the understanding of this novel synthetic avenue based on kinetically driven liquid chemistries.

Compared with previously reported approaches based on plasma-induced liquid chemistry (where an additional chemical component was always used to stabilize the NPs), our work demonstrate that plasma-only chemistry can both reduce and stabilize NPs. Therefore we have considerably progressed from a hybrid plasma/wet chemistry approach to a fully plasma-enabled approach resulting in a largely simpler, more rapid and cleaner method that can greatly facilitate the subsequent surface functionalization of AuNPs. Moreover, the availability of surfactant-free NPs opens up a range of new functionalization opportunities that would not be otherwise available because precluded by specific surface chemistries. The use of electrostatic stabilization also provides opportunities for controlled aggregations which can potentially lead to self-organization mechanisms useful for a range of applications (e.g. inter-/intra-coupling plasmonics, conductive NPs chains for sensing etc). Furthermore, this method can be easily implemented in a continuous flow process, compared to batch-based chemical synthesis, which would bring about unprecedented and industrially viable nanomanufacturing capabilities. Overall, the features offered by this microplasma–liquid system could allow the synthesis to be highly environmentally friendly, low cost and accessible to a wide range of non-specialist users.

It should be noted that preliminary results on this work were previously reported [36] and a partial summary of our findings are published in an invited feature paper [37]. However in this contribution we provide a full account of this work including an in-depth analysis of the plasma-induced mechanisms leading to NPs formation.

2. Results

2.1. Plasma-induced non-equilibrium liquid chemistry (PiLC)

In order to synthesize surfactant-free AuNPs, an atmospheric pressure microplasma is generated at the surface of a gold (III)-chloride-trihydrate ($HAuCl_4{\cdot}3H_2O$) aqueous solution (0.05–1 mM $HAuCl_4$ concentration; figure 1). The interactions of the gas-phase plasma with the solution initiate liquid-based reactions that determine the nucleation and growth of AuNPs from the reduced gold precursor ($HAuCl_4$). The plasma–liquid interface is possibly represented by a gas/water vapour plasma environment where electrons are believed to be responsible for initiating reactions that then cascade into the liquid solution (see supporting information available at stacks.iop.org/Nano/24/245604/mmediaand [37] for a more detailed discussion on the plasma characteristics). More specifically, the plasma is generated across a ∼0.7 mm gap between the liquid surface and a stainless steel capillary (1 mm external diameter and 0.25 mm internal diameter). Inside the capillary, helium is flown at 25 standard cubic centimetres (sccm) so that the microplasma is largely formed in helium gas. The microplasma setup is shown in figure 1. The microplasma is sustained by a high dc voltage (up to 2 kV) applied at the carbon rod while the stainless steel capillary is grounded through a ballast resistor of 100 kΩ (see figure 1). The processing current is maintained constant (1–5 mA) while the applied voltage varies (due to changes in the solution conductivity) from about 2 kV at the start of the

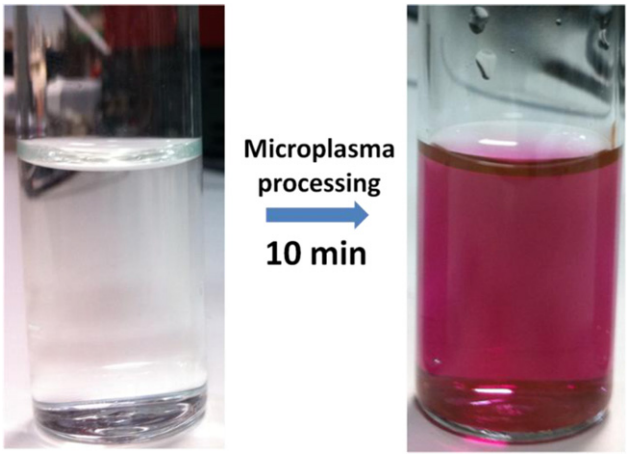

Figure 2. Colour change of the 0.2 mM $HAuCl_4$ aqueous solution after 10 min microplasma treatment. The change in the colour of the solution is due the formation of gold nanoparticles that exhibit a typical resonance absorption peak with the resulting visible purple colour.

treatment down to about 800 V after 10 min processing. The temperature of 20 ml water exposed to the plasma sustained by a 5 mA current for 10 min was observed to increase from about 16 to about 36 °C. Similar observation were done at different conditions were the temperature never increased above 40 °C.

2.2. Synthesis of gold nanoparticles

Microplasma processing of a 0.2 mM $HAuCl_4$ aqueous solution at 5 mA induces a change in the colour of the solution within a few minutes (see figure 2), which indicates the formation of AuNPs. UV–vis absorption spectroscopy was used initially to verify the presence of AuNPs after 10 min processing. The absorption measurements exhibited a peak at 544 nm which is due to typical plasmon resonance effects of AuNPs. The reaction mechanisms that lead to the salt reduction, AuNPs nucleation and growth will be discussed later in this manuscript. In order to confirm the synthesis and characteristics of the AuNPs, a detailed TEM analysis was conducted. TEM images show that microplasma processing produces particles with a distribution of different shapes and size. In particular, from TEM images it is possible to observe particles with a range of two-dimensional projections, i.e. spherical, hexagonal and triangular (see figure 3 and supporting information available at stacks.iop.org/Nano/24/245604/mmedia). The diameter of the NPs produced at these conditions ranges from about 7 to about 60 nm (also, see figure 3 and supporting information available at stacks.iop.org/Nano/24/245604/mmedia); it can also be observed that these are often multiply twinned NPs as it is frequently observed for AuNPs of corresponding sizes synthesized with a variety of techniques [38–41].

TEM images can only reveal the two-dimensional projections of particles, however, for simplicity of the discussion we will refer to the two-dimensional projection as particle shape. At these processing conditions, the most frequent shapes are spherical (58%) and hexagonal (36%) shapes (figure 3(c)). The synthesis process also formed some triangular and cubical particles with some rod-shaped particles which contributed to a smaller fraction of the total population (figure 3(c)). Figure 3(d) illustrates the particle size distribution where the average is found to be 35 nm, determined by fitting the experimental size distribution with a Gaussian function; the size of the particles corresponds to the diameter for spherical particles while the particle's longest length is considered for other shapes. The analysis of the TEM images involved more than 350 particles produced at 0.2 mM $HAuCl_4$ concentration. In the next sections the effects of changing the gold precursor concentration and the processing plasma current will be analysed. These results will contribute to provide a description of the reaction mechanisms that are believed to be responsible for the synthesis of AuNPs via kinetic-driven processes.

2.3. Effect of precursor concentration on the particle size and shape distributions

Here we compared the AuNP synthesis by varying the gold precursor concentration while keeping constant the processing current at 5 mA. Figure 4(a) compares the colour of the solutions after 10 min processing for different initial $HAuCl_4$ concentrations (2.5 μM, 0.05, 0.1, 0.2, 0.6 and 1 mM). It is clearly observed that different precursor concentrations form colloids with different optical properties (see supporting information available at stacks.iop.org/Nano/24/245604/mmediafor the full range of photos at different processing current values).

The visible optical properties are reflected in the UV–vis absorption spectra (figure 4(b)), where the resonant absorption peaks are observed for all samples (see supporting information available at stacks.iop.org/Nano/24/245604/mmediafor the full range of absorption spectra at different processing conditions). Figure 4(b) indicates that the initial molar concentration of the precursor affects the absorption resonant peak wavelength of the plasma-processed solution. The absorption resonant peak position shifts from 532 nm (2.5 μM) to 581 nm (1 mM) and is in agreement with the surface plasmon resonance (SPR) of gold nanoparticles [16]. It is widely reported that SPR wavelength is affected by various parameters such as particle shape and size, dielectric properties of the solvent, surface functionalization and aggregate morphology [16, 42–47]. In particular, figure 4(b) may suggest that the precursor concentration could be used to control the size of the synthesized NPs [13].

This is confirmed by the average NPs sizes of the samples produced at different precursor concentrations (figure 5); the average sizes were determined by TEM analysis following the same procedure as described in the previous section and for each synthesis at each different concentration, more than 150 NPs were analysed in each case. It should be noted that at a concentration of 5 mM we observed the formation of connected columnar structures with no optical resonance properties (see figure S1(f) in the supporting information available at stacks.iop.org/Nano/24/245604/mmedia).

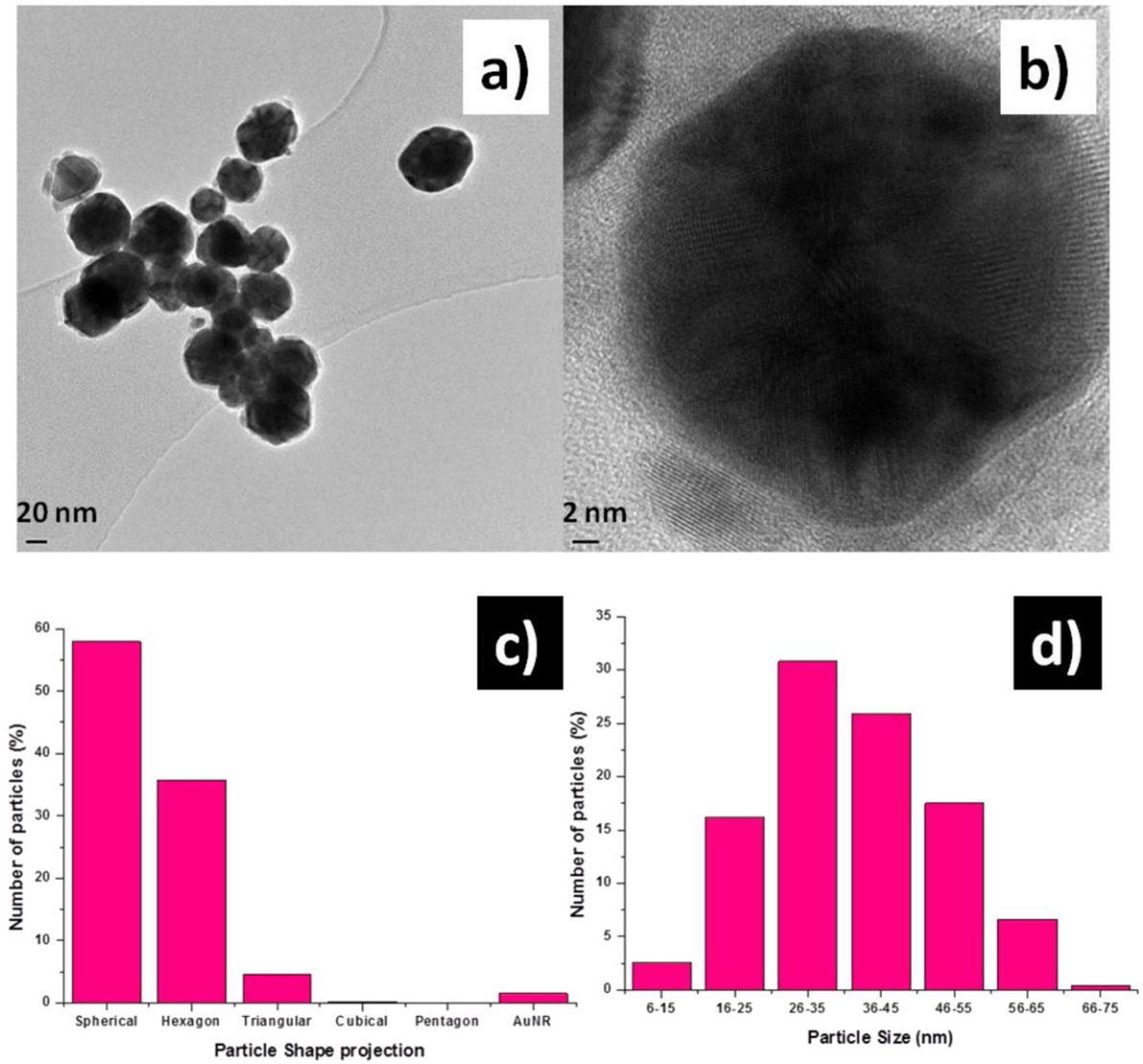

Figure 3. (a) and (b) Representative transmission electron microscope (TEM) images of the gold nanoparticles (AuNPs) synthesized from a 0.2 mM $HAuCl_4$ aqueous solution. AuNPs shape (c) and size (d) distribution resulted from the analysis of TEM images.

TEM analysis was also used to determine the particle shape distributions (figure 6) for the same set of five processing conditions as above (i.e. 2.5 μM, 0.05, 0.1 and 1 mM gold precursor concentrations and processed at a discharge current of 5 mA; see also figure 3(d) for the distribution corresponding to a concentration of 0.2 mM). According to the literature, competition between nucleation and growth at different facets determines the size and shape of metal nanoparticles in solutions [48]. At low molar concentrations (2.5 μM) all the particles are spherical. For medium molar concentrations (0.05 and 0.1 mM) the particle shape distribution includes various shapes of AuNPs such as spherical, hexagonal, pentagonal, triangular, etc with some gold nanorods. At higher molar concentrations (0.2 and 1 mM) more than 80% of the AuNPs were found to be spherical or hexagonal. The predominance of given shapes at different concentrations may indicate that reduction of the gold precursor is activated differently for the different conditions. For instance, at low concentration (e.g. 2.5 μM) reduction may be occurring predominantly in bulk solution, i.e. $HAuCl_4$ molecules may be reduced to yield Au^0 atoms. It follows that the aggregation of reduced atoms is isotropic leading to spherical particles. When the concentration of the precursor is higher (0.05, 0.1, 0.2 and 1 mM), the probability of partially reduced $HAuCl_4$ to interact with growing NPs is higher leading to reduction on the surface of existing nucleated seeds (or small particles); surface-assisted reduction will be at some extent dependent of the surface energy of the different crystal facets possibly leading to non-spherical shapes.

2.4. Control of reaction rates through the plasma processing current

The current of plasma processing affects the particles formation process. Figure 7 shows typical absorption spectra of 1 mM solutions processed by different discharge currents (see supporting information available at stacks.iop.org/Nano/

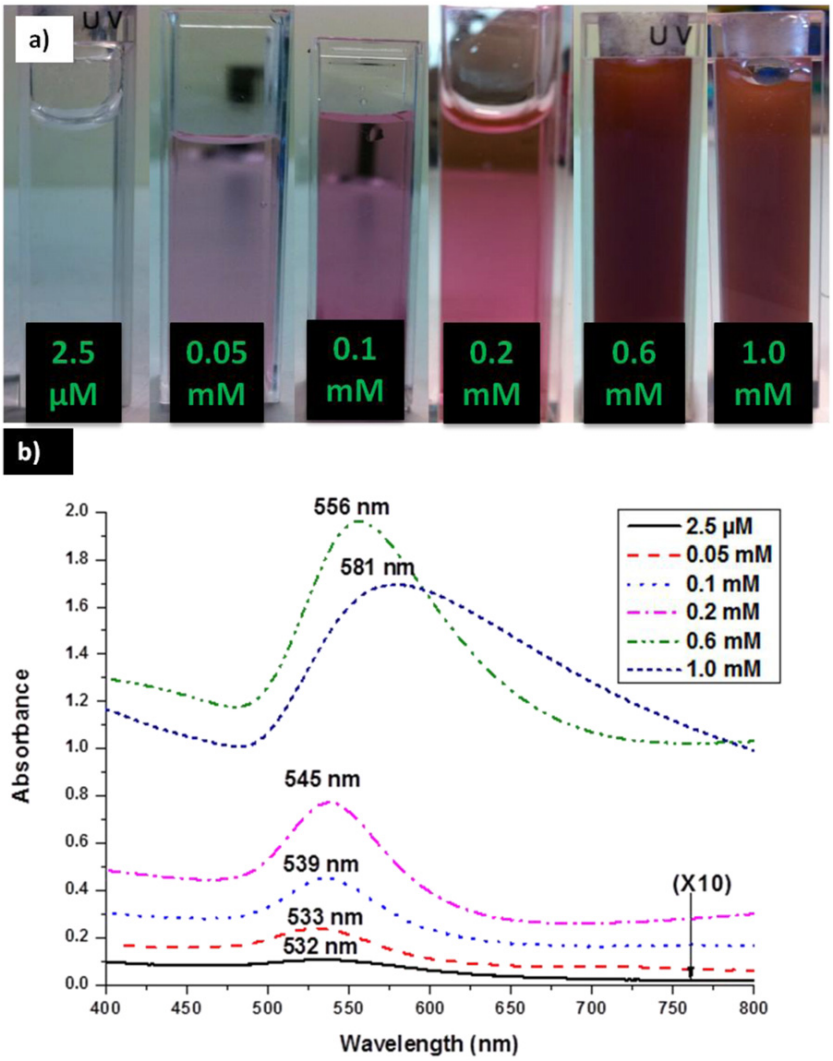

Figure 4. Six different $HAuCl_4$ concentrations (2.5 μM–1 mM) processed by microplasma at a current of 5 mA. (a) Colour of the solutions after 10 min of microplasma processing and (b) corresponding absorption spectra that exhibit different resonance peaks for different concentrations of $HAuCl_4$ (note that the intensity of the absorption spectrum for the 2.5 μM sample is multiplied here by 10 for clarity).

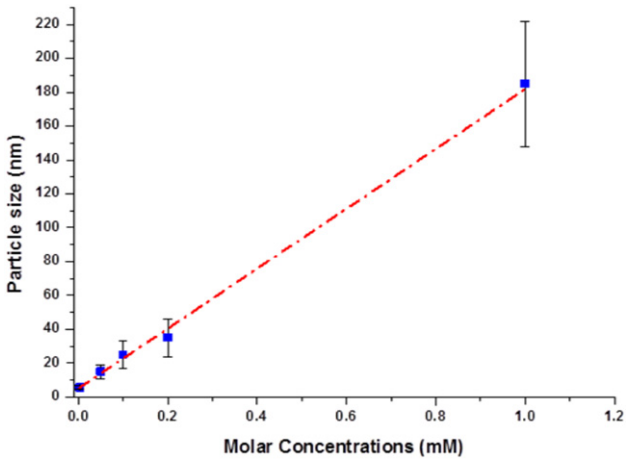

Figure 5. Variation of particle size resulted from different concentrations of $HAuCl_4$. Particle size increases with increasing the molar concentration. The dashed red line represents the linear fit to all the five points of the curve. The results reported in this figure were for the major part previously published [38].

24/245604/mmediafor the full range of absorption spectra at different processing conditions). It can be observed here that by increasing the discharge current, (from 1 to 5 mA) the peak wavelength does not change and we can deduce that the discharge current affects the synthesis rate and therefore the number of particles synthesized within the 10 min processing. However, control of the reaction rate is also determined and limited by the concentration of the initial gold precursor concentration [37].

2.5. Size-dependent optical properties of the synthesized AuNPs

We have also compared the variation of the plasmon resonance wavelength (PRW) and bandwidth (PRB) as a function of particles size which were produced with different precursor concentrations as previously described (see figure 8). Figure 8 shows that the PRW increases with increasing average particle size while the PRB increases with average size above ∼15 nm. When particles are smaller than

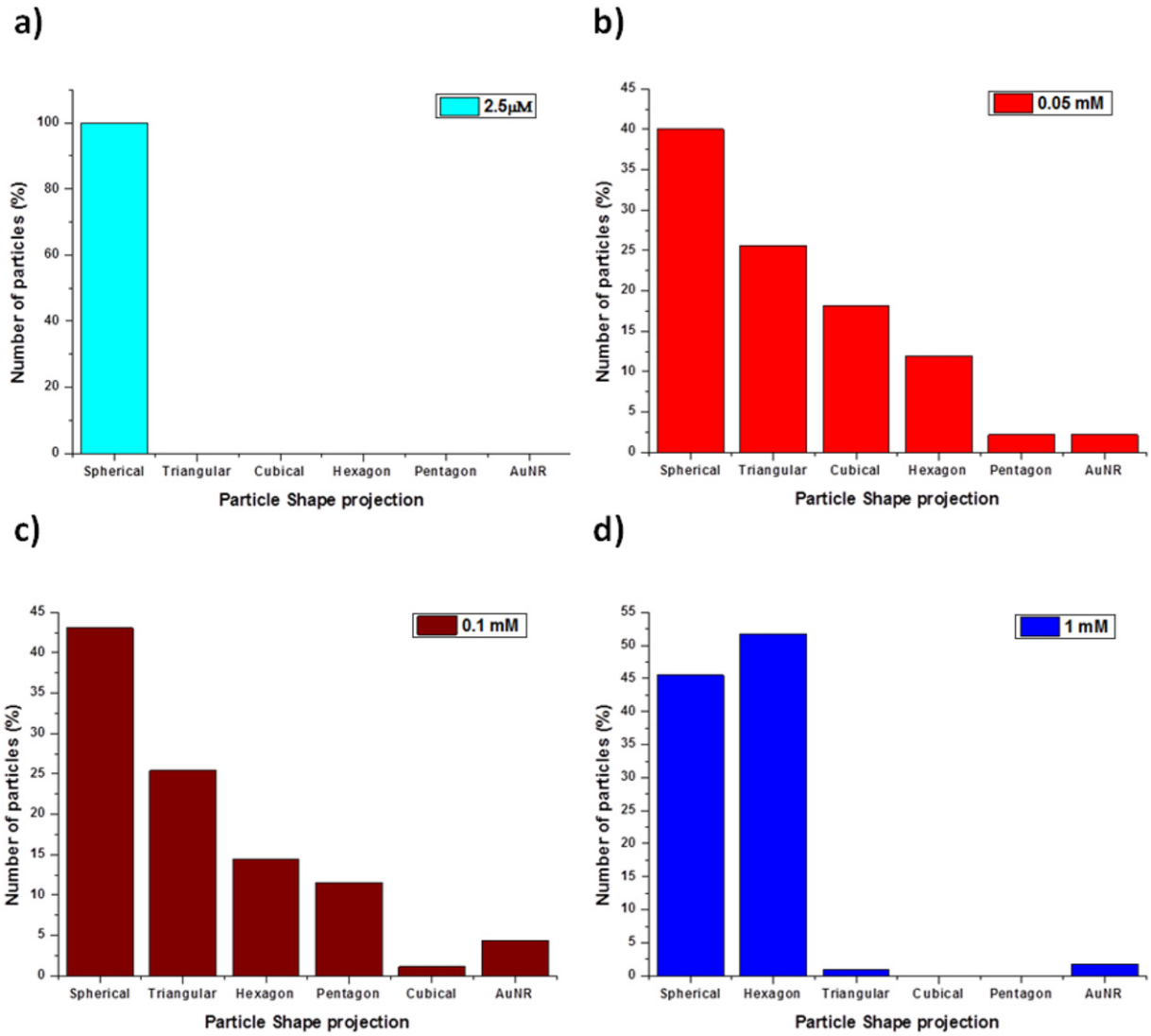

Figure 6. Transmission electron microscopy (TEM) analysis of (a) 2.5 μM (b) 0.05 mM, (c) 0.1 mM and (d) 1 mM $HAuCl_4$ solutions processed by microplasma at 5 mA discharge current (see also figure 3(c) for the distribution corresponding to a concentration of 0.2 mM).

15 nm, the PRB is seen to increase again. These results are in agreement with plasmon resonance measurements of AuNPs (see for instance [49, 50]). PRB was determined as the full width at half maximum of the resonant peak from the absorption spectra corresponding to each particular $HAuCl_4$ molar concentration (and therefore the measured average particle size); PRB depends on a range of parameters such as the average size, the size distribution, shape etc. While a range of factors may have contributed to the PRB for each synthesis condition, figure 8(b) may indicate the existence of an intrinsic and extrinsic region for AuNPs with respect to the PRB [49, 50].

3. Discussion

3.1. Description of the plasma-induced chemistry leading to AuNP synthesis

Liquid chemistry initiated by microplasma at the plasma–liquid interface is ultimately responsible for the nucleation and corresponding synthesis of AuNPs in liquid. Several studies have reported on the reaction mechanisms leading to AuNP synthesis from the reduction of $HAuCl_4$ in aqueous solution; salt reduction was generally attributed to plasma electrons [14, 16, 36, 51, 52], hydrogen radicals in liquid [15, 17, 20, 52–54], hydrated electrons e_{aq}^- [13, 17] and hydrogen peroxide [55]. However, NPs synthesis by plasma-induced chemistry is still largely unexplained. In order to clarify some of the aspects involved in the plasma-induced synthesis of the AuNPs in liquid we have performed a more in-depth analysis of the related chemistry.

Firstly, we demonstrate that interactions at the plasma–liquid interface are essential for the surfactant-free synthesis of AuNPs. We performed direct electrochemistry of the $HAuCl_4$ aqueous solution with two electrodes both immersed in solution. We applied the same electrical conditions that were used for the plasma-based AuNPs synthesis reported above; however the formation of NPs was not observed in this case confirming that plasma-induced

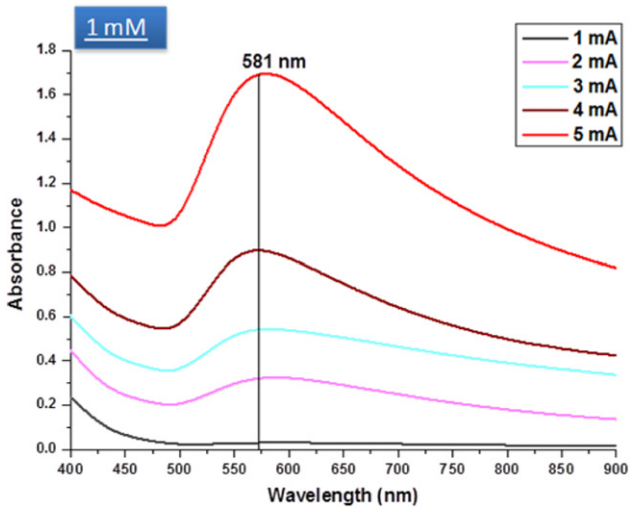

Figure 7. Typical absorption spectra of 1 mM $HAuCl_4$ solutions processed by five different discharge currents namely 1, 2, 3, 4 and 5 mA (see supporting information available at stacks.iop.org/Nano/24/245604/mmediafor the full range of absorption spectra at different processing conditions).

reactions are essential for reducing the gold precursor and are fundamentally different from reactions promoted with a standard electrochemical cell arrangement.

Secondly, we wanted to better understand the role of water in the synthesis of AuNPs, therefore we tried to synthesize AuNPs by plasma-induced liquid chemistry using $HAuCl_4$ in ethanol. However, the use of ethanol as a solvent prevented the formation of AuNPs implying that plasma-induced reactions specifically with water represented fundamental steps for achieving AuNP synthesis.

In order to identify the radical species formed at the plasma–liquid interface, we performed a range of supporting measurements such as pH and conductivity measurements (not shown here). In general, plasma processing of the $HAuCl_4$ aqueous solution decreases the pH value, from about 3.8 to 3.4 and increases the overall solution conductivity from 0.09 to about 0.17 mS cm^{-1}. Reduced pH and increased conductivity are believed to be the consequence of water oxidation at the anode (the carbon rod in figure 1) where, due to the very high applied potential, a copious amount of H^+ is produced [37].

From our previous work, we know that hydrogen peroxide is formed in our plasma–water system [37]. The formation of H_2O_2 is key to understanding this hybrid plasma-chemical synthesis process because hydrogen peroxide has been reported as a reducing agent for the gold precursor [55]. Also, because hydrogen peroxide is not formed in a standard electrochemical approach with both electrodes immersed in solution, this suggests that plasma electrons accelerated at the plasma–water interface are responsible for the formation of H_2O_2. From previous studies the contribution of other radicals, ions and photons from the plasma can be neglected in this specific configuration [23, 37, 51, 56]. A complete qualitative analysis of the possible reactions [37, 57] leads to the following being identified as the primary chemical pathways for H_2O_2 production

$$e^-_{gas} + H_2O \rightarrow OH^\bullet + H^-, \quad \text{plasma–liquid interface reaction} \tag{1}$$

$$2OH^\bullet \rightarrow H_2O_2, \quad \text{bulk liquid reaction} \tag{2}$$

where the first reaction represents dissociative electron attachment in the vicinity of the liquid/vapour water interface by electrons from the plasma. In reaction (1), the H^- is essentially a 'by-product' that has a very short lifetime and therefore is believed to quickly react with water molecules without participating to the reaction chemistry leading to AuNP synthesis. On the other side, OH that has a lifetime in the nanosecond range can quickly react to produce H_2O_2, the latter with a lifetime of several days. Free electrons that do not contribute to reaction (1) and reach the bulk of the liquid,

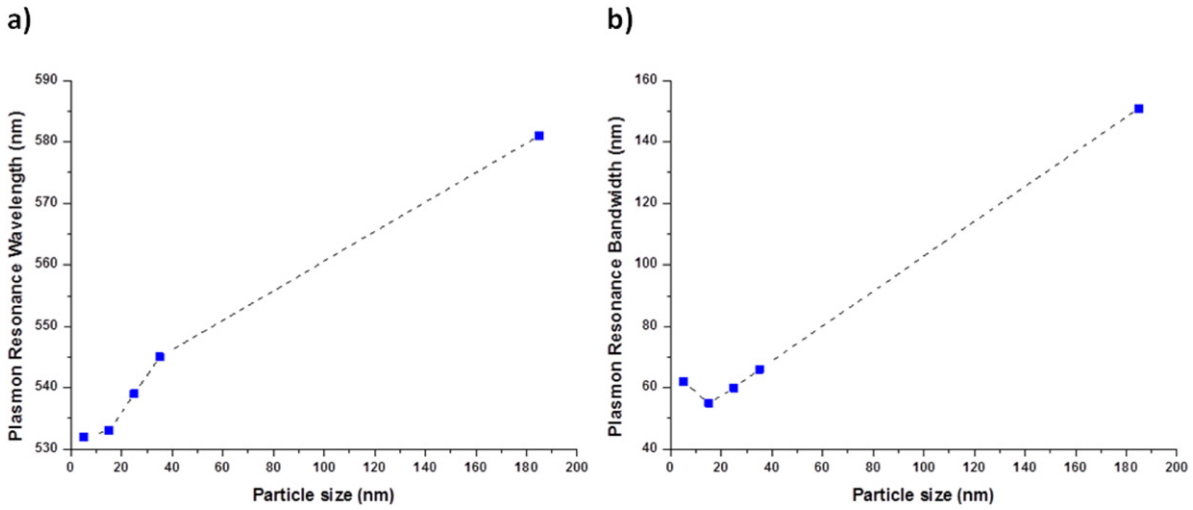

Figure 8. Plasmon resonance wavelength (a) and bandwidth (b) plotted as a function of the measured average particle size synthesized with different precursor concentrations. The results reported in this figure were for the major part previously published [38].

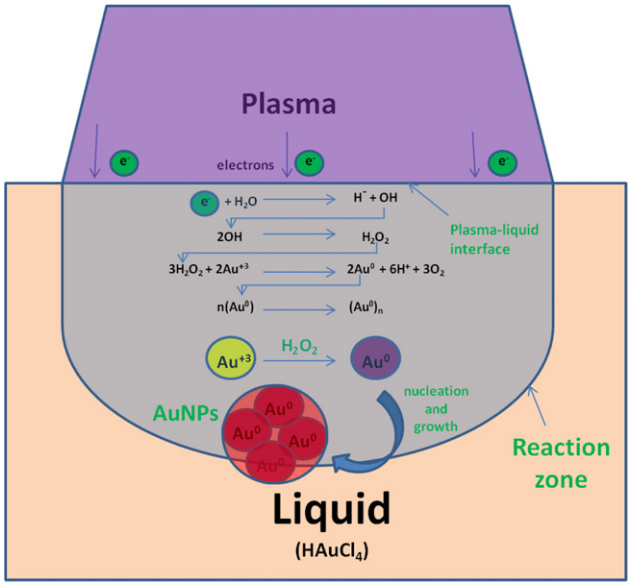

Figure 9. A schematic model of reaction mechanisms for the gold nanoparticles synthesis by plasma-induced liquid chemistry.

will thermalize and hydrate, i.e. bound to water molecules; on sub-nanosecond timescales, hydrated electrons and water could only produce OH^- and $H^\bullet$. It follows that reactions (1) and (2) above are the most probable mechanism that lead to hydrogen peroxide formation. Therefore our hypothesis is that electrons do not directly reduce the gold salt, rather electron-induced reactions at the plasma–liquid interface promote cascaded chemistry leading to hydrogen peroxide (via equations (1) and (2) above) and that the latter reduces the gold precursor via

$$3H_2O_2 + 2Au^{+3} \rightarrow 2Au^0 + 6H^+ + 3O_2 \qquad (3)$$

with consequent nucleation and growth of the AuNPs (see figure 9).

However, while the above reduction reaction (3) has been reported before [55] in the literature, we have observed that this reduction reaction requires the presence of water because we could not synthesize AuNPs in an ethanol-based solution, even though we have confirmed that H_2O_2 was produced also in this case. Therefore, reaction (3) cannot be the main reducing channel as water molecules or corresponding ions (OH^- or H^+) should play a role in the reduction of the gold precursor. Therefore we suggest here that a more plausible reaction could be

$$3H_2O_2 + 3OH^- + Au^{+3} \rightarrow Au^0 + 3HO_2 + 3H_2O. \qquad (4)$$

In support of our hypotheses we have measured the hydrogen peroxide concentration in the solution using a reaction with a titanium-based scavenger (titanium(IV) oxysulfate–sulfuric acid), hereafter referred to as Ti–S, which forms yellow complex cations that can then be detected by UV–vis spectroscopy in the region between 400 and 450 nm [58]. This required a series of experiments. From figures 10(a) and (b) (sample A and B) it is clear that, in the wavelength region used for H_2O_2 detection, the Ti–S absorption spectra for water without the gold precursor added is independent of when the Ti–S is added and that the Ti–S compound was not affected by exposure to the plasma.

The identical procedure was then used with $HAuCl_4$ aqueous solutions (sample C and sample D in figure 10(a)). The UV–vis absorption spectra of these two samples are also shown in figure 10(b) and show different optical characteristics. In the case of sample C, the absorption at the PRW indicates the presence of AuNPs; also, absorption around 407 nm suggests the presence of hydrogen peroxide. However, sample D does not present any absorption at the PRW and still presents absorption related to hydrogen peroxide. The comparison of sample C and D confirms that the gold salt is reduced by hydrogen peroxide.

In sample C, H_2O_2 is formed during plasma processing so that the latter can freely reduce $HAuCl_4$ and allow

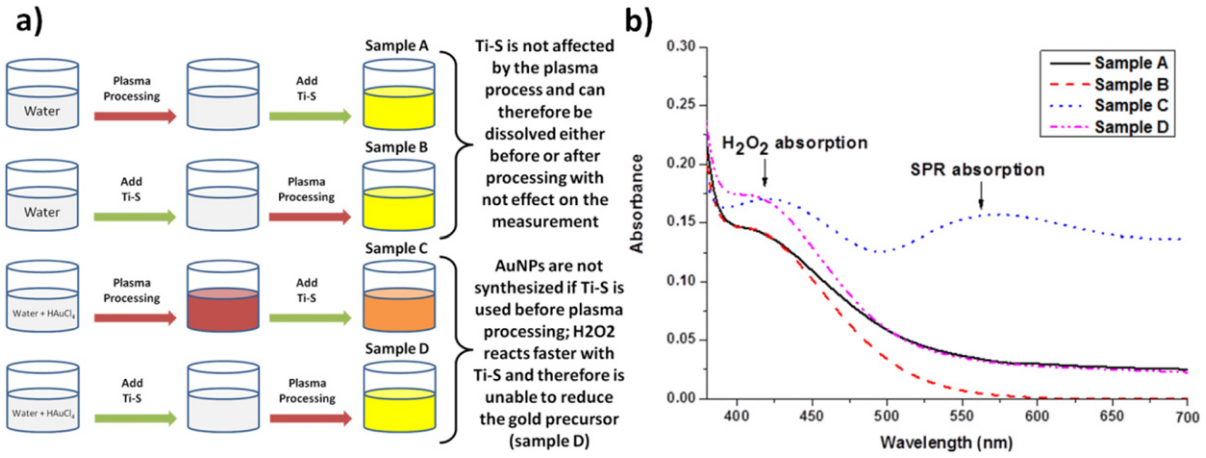

Figure 10. (a) Methodology used to determine the effect of the plasma exposure on titanium(IV) oxysulfate–sulfuric acid (Ti–S) compound (samples A and B) and to verify the role of hydrogen peroxide on the gold salt reduction (sample C and D). (b) Measurements indicating absorption at ∼407 nm related to the reaction of the Ti–S compound with H_2O_2 and also the typical plasmon resonance absorption above 500 nm due to the presence of gold nanoparticles.

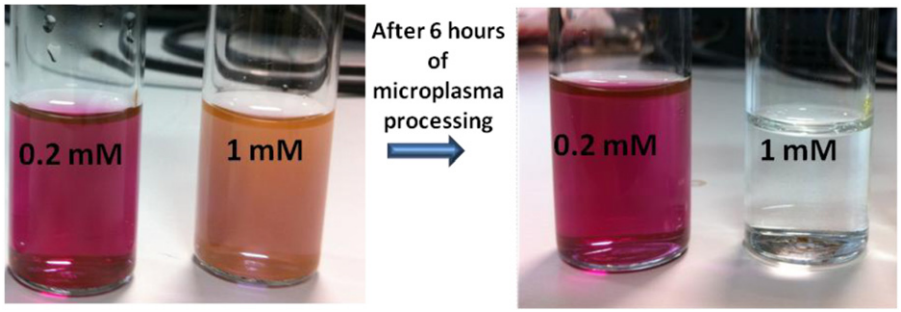

Figure 11. Photographs of gold nanoparticle colloids synthesized from 0.2–1 mM solutions processed at 5 mA current. The photos compare the colour of the samples straight after (left) and 6 h after (right) the microplasma processing.

the synthesis of AuNPs. However in sample D, the H_2O_2 produced by the plasma processing is reduced by the Ti–S and is therefore not present to reduce $HAuCl_4$ and allow the synthesis of AuNPs. When Ti–S is added later to sample C after the AuNPs have been synthesized, it reacts with the remaining H_2O_2.

These results are strong evidence in support of our hypotheses and explain the synthesis of surfactant-free AuNPs utilizing a novel plasma-based approach. They are also significant for a much broader range of plasma-induced liquid chemistry applications. Further studies will be however required to fully understand the kinetics and provide a complete picture of plasma-induced mechanisms also in consideration that for reaction (3) to take place water may be required and that reaction (4) might be effectively taking place.

3.2. Additional comments on the AuNPs shapes and on the colloids stability

The presence of different shapes in the NPs distribution of figure 6 could be due to different spatial processing conditions in the solution; this is an aspect that at the moment is very little controlled in our setup and improvements in the configuration (e.g. using fluidic channels) could provide great opportunities for controlling the morphology through kinetic avenues. However, an in-depth study needs to be carried out in order to understand the formation of different AuNPs morphologies; for instance when processing the solution with 1 mM concentration, spherical and hexagonal particles seem to be the preferred shapes while a wider range of morphologies are observed for 0.05–0.1 mM precursor concentrations (figures 3(c) and 6).

The stability of the AuNPs in solution has always been an important issue for some applications. The results reported in the previous sections are based on measurements taken shortly after processing (<5 min); however we have observed the stability of our AuNP colloids for a minimum of 6 h and up to several months and with samples that have now been stable for more than a year and currently still stable (see supplementary information available at stacks.iop.org/Nano/24/245604/mmedia). In order to provide some insights into the control of AuNPs stability, figure 11 compares the photographs of two different molar concentrations (0.2–1 mM) straight after processing and after 6 h storage. Both samples show characteristic orange/purple colour soon after processing indicating the presence and dispersion of the AuNPs in the solution. However, it can be noted that the 0.2 mM sample does not change in colour after 6 h storage whereas the 1 mM sample becomes transparent. Furthermore the 1 mM sample exhibits aggregated structures at the bottom of the vial, which means that the lower concentration forms, in this case, the most stable AuNPs. We believe that this is due to the electrostatic stabilization provided by plasma which seems to be confirmed by our zeta potential measurements after processing which consistently show negative values below −30 mV. The electrostatic stabilization largely depends on processing parameters but is also dependent on storage conditions (e.g. material of the storing container, see supporting information available at stacks.iop.org/Nano/24/245604/mmedia) and at this time we have not produced an in-depth study of zeta potential measurements over time (which is complicated by required measurement parameters such as viscosity for partially consumed gold precursor concentration). However, we can speculate that electrons 'injected' from the plasma through the plasma–liquid interface may contribute to negatively charge the surface of the AuNPs. Because electrons indirectly participate to the reduction of the Au precursor, at a constant processing current (figure 11), a lower precursor concentration allows for a larger surface charge to be accumulated on the AuNPs. In other words electrons that do not induce hydrogen peroxide formation through reactions (1) and (2), will necessary tend to be captured by the metal character of the gold nanoparticles; hence AuNPs produced with lower initial precursor concentrations will exhibit enhanced stability due to Coulomb repulsion (figure 11) and similarly stable AuNPs can be produced by increasing the processing current. Therefore, our initial results show that the discharge current represents a control parameter to produce from highly stable AuNPs colloids to AuNPs where aggregation can be controlled over time. However as mentioned previously and as shown in the supporting information (available at stacks.iop.org/Nano/24/245604/mmedia), the storage conditions can either improve or degrade the stability of AuNPs. While the processing and storage conditions that lead to stable colloids (>1 yr) have been already identified, both aspects of controlled NPs

morphology and controlled electrostatic stabilization still require further experimentations and will be the focus of further study that will be reported in the future.

4. Experimental section

4.1. Methods

A solid powder of gold(III) chloride trihydrate ($HAuCl_4 \cdot 3H_2O$) was purchased from Sigma Aldrich (UK) to obtain the aqueous solutions of different molar concentrations. Six different molar concentrations namely 2.5 μM, 0.05, 0.1, 0.2, 0.6 and 1 mM were prepared by dissolving a proper amount of gold salt with distilled water. Each solution was treated by plasma for different currents (1–5 mA) for the period of 10 min. Titanium(IV) oxysulfate–sulfuric acid solution was purchased from Sigma Aldrich (UK). It is generally used for the detection of H_2O_2 and ether peroxides. We have used this chemical for the measurements of H_2O_2 in our setup by using the method reported by Lukeš [58]. Reaction of H_2O_2 with titanyl ions gives yellow-coloured complex of pertitanic acid which can be detected by measuring its absorption at ∼407 nm. Titanium sulfate reagent was mixed with water and $HAuCl_4$ aqueous solutions before and after plasma treatment and finally absorbance of the resulting solution was measured by UV–vis spectroscopy.

4.2. Instrumentation

TEM with a Philips CM 100 and JEOL JEM-2100F was performed to measure the particle size. Perkin Elmer's LAMBDA 35 UV–vis spectroscopy was used to determine the absorption characteristics of the As-synthesized gold nanoparticles.

5. Conclusions

AuNPs of various sizes are successfully synthesized by plasma-induced non-equilibrium liquid chemistry without using any surfactants or stabilizers which demonstrates the versatility of this technique. Lower precursor concentrations form the smaller AuNPs and increasing the current of plasma processing accelerate the particle formation process and hence the number density of AuNPs in solution. Reaction mechanisms for AuNP synthesis are discussed and provide an interesting description of plasma-induced liquid chemistry. It is concluded that hydrogen peroxide is playing the role of reducing agent to synthesize AuNPs and allows the formation of electrostatically stable NPs without any need of surfactants/stabilizing molecules. The results also emphasize that reaction at the plasma–liquid interface are essential to drive this kinetically driven synthesis process. The analysis of the plasma-induced chemical reactions provides important results that will contribute to further developments in plasma-induced liquid chemistry for nanomaterials synthesis and functionalization. Furthermore the results presented here contribute to a broader understanding of plasma–liquid interactions in general and for the very wide range of potential applications.

Acknowledgments

This work on gold nanoparticles is supported by the University of Ulster Strategic Fund. JP acknowledges the University of Ulster Vice-Chancellor Research Studentship for financial support. The authors would like to thank Stephen McFarland (Queen's University Belfast, UK) and Calum Dickinson (University of Limerick, Ireland) for the TEM analysis of the gold nanoparticles. The authors are also thankful to many useful discussions with Steffan Cook (Cardiff University—UK/University of Ulster—UK).

References

[1] Arvizo R, Bhattacharya R and Mukherjee P 2010 *Expert Opin. Drug Deliv.* **7** 753–63
[2] Sperling R A, Gil P R, Zhang F, Zanella M and Parak W J 2008 *Chem. Soc. Rev.* **37** 1896–908
[3] Huang X, Jain P K, El-Sayed I H and El-Sayed M A 2007 *Nanomedicine* **2** 681–93
[4] Ghosh P, Han G, De M, Kim C K and Rotello V M 2008 *Adv. Drug Deliv. Rev.* **60** 1307–15
[5] Madu A, Njoku P, Iwuoha G and Agbasi U 2011 *Int. J. Phys. Sci.* **6** 635–40
[6] Gan P P, Ng S H, Huang Y and Li S F Y 2012 *Bioresour. Technol.* **113** 132–5
[7] Amendola V, Rizzi G A, Polizzi S and Meneghetti M 2005 *J. Phys. Chem.* B **109** 23125–8
[8] Mariotti D and Sankaran R M 2010 *J. Phys. D: Appl. Phys.* **43** 323001
[9] d'Agostino R, Favia P, Oehr C and Wertheimer M R 2005 *Plasma Process. Polym.* **2** 7–15
[10] Nozaki T and Okazaki K 2006 *Pure Appl. Chem.* **78** 1157–72
[11] Laroussi M and Lu X 2005 *Appl. Phys. Lett.* **87** 113902
[12] Mariotti D and Sankaran R M 2011 *J. Phys. D: Appl. Phys.* **44** 174023
[13] Liang X, Wang Z and Liu C 2010 *Nanoscale Res. Lett.* **5** 124–9
[14] Zou J J, Zhang Y and Liu C J 2006 *Langmuir* **22** 11388–94
[15] Saito N, Hieda J and Takai O 2009 *Thin Solid Films* **518** 912–7
[16] Kim S M, Kim G S and Lee S Y 2008 *Mater. Lett.* **62** 4354–6
[17] Chen Q, Kaneko T and Hatakeyama R 2011 *Chem. Phys. Lett.* **521** 113–7
[18] Chiang W H, Richmonds C and Sankaran R M 2010 *Plasma Sources Sci. Technol.* **19** 034011
[19] Sivaraman S K, Kumar S and Santhanam V 2010 *Gold Bull.* **43** 275–86
[20] Furuya K, Hirowatari Y, Ishioka T and Harata A 2007 *Chem. Lett.* **36** 1088–9
[21] Nozaki T, Sasaki K, Ogino T, Asahi D and Okazaki K 2007 *Nanotechnology* **18** 235603
[22] Sankaran R M, Holunga D, Flagan R C and Giapis K P 2005 *Nano Lett.* **5** 537–41
[23] Švrček V, Mariotti D and Kondo M 2010 *Appl. Phys. Lett.* **97** 161502
[24] Becker K, Schoenbach K and Eden J 2006 *J. Phys. D: Appl. Phys.* **39** R55
[25] Tachibana K 2006 *IEEJ Trans. Electr. Electron. Eng.* **1** 145–55
[26] Sankaran R M and Giapis K P 2001 *Appl. Phys. Lett.* **79** 593–5
[27] Ito T, Izaki T and Terashima K 2001 *Thin Solid Films* **386** 300–4
[28] Sankaran R M and Giapis K P 2002 *J. Appl. Phys.* **92** 2406

[29] Shimizu Y, Sasaki T, Ito T, Terashima K and Koshizaki N 2003 *J. Phys. D: Appl. Phys.* **36** 2940
[30] Mariotti D 2008 *Appl. Phys. Lett.* **92** 151505
[31] Chiang W H and Sankaran R M 2007 *Appl. Phys. Lett.* **91** 121503
[32] Wagner J and Köhler J 2005 *Nano Lett.* **5** 685–91
[33] Yen B K H, Günther A, Schmidt M A, Jensen K F and Bawendi M G 2005 *Angew. Chem. Int. Edn* **117** 5583–7
[34] Richmonds C and Sankaran R M 2008 *Appl. Phys. Lett.* **93** 131501
[35] Sau T K, Rogach A L, Jäckel F, Klar T A and Feldmann J 2010 *Adv. Mater.* **22** 1805–25
[36] McKenna J, Patel J, Mitra S, Soin N, Švrček V, Maguire P and Mariotti D 2011 *Eur. Phys. J.: Appl. Phys.* **56** 24020
[37] Mariotti D, Patel J, Švrček V and Maguire P 2012 *Plasma Process. Polym.* **9** 1074–85
[38] Pal A 2004 *Mater. Lett.* **58** 529–34
[39] Vitale F, Fratoddi I, Battocchio C, Piscopiello E, Tapfer L, Russo M V, Polzonetti G and Giannini C 2011 *Nanoscale Res. Lett.* **6** 103
[40] Link S, Burda C, Wang Z L and El-Sayed M A 1999 *J. Chem. Phys.* **111** 1255–64
[41] Sun Y and Xia Y 2002 *Science* **298** 2176–9
[42] Philip D 2008 *Spectrochim. Acta,* A **71** 80–5
[43] Sharma P, Brown S, Walter G, Santra S and Moudgil B 2006 *Adv. Colloid Interface Sci.* **123** 471–85
[44] Jain P K, Lee K S, El-Sayed I H and El-Sayed M A 2006 *J. Phys. Chem.* B **110** 7238–48
[45] El-Brolossy T, Abdallah T, Mohamed M B, Abdallah S, Easawi K, Negm S and Talaat H 2008 *Eur. Phys. J.: Spec. Top.* **153** 361–4
[46] Yu K, Kelly K L, Sakai N and Tatsuma T 2008 *Langmuir* **24** 5849–54
[47] Haiss W, Thanh N T K, Aveyard J and Fernig D G 2007 *Anal. Chem.* **79** 4215–21
[48] Sakai T, Enomoto H, Torigoe K, Sakai H and Abe M 2009 *Colloids Surf.* A **347** 18–26
[49] Link S and El-Sayed M A 1999 *J. Phys. Chem.* B **103** 4212–7
[50] Link S and El-Sayed M A 2000 *Int. Rev. Phys. Chem.* **19** 409–53
[51] Lee S W, Liang D, Gao X and Sankaran R M 2011 *Adv. Funct. Mater.* **21** 2155–61
[52] Kaneko T, Baba K and Hatakeyama R 2009 *Plasma Phys. Control. Fusion* **51** 124011
[53] Hieda J, Saito N and Takai O 2008 *J. Vac. Sci. Technol.* A **26** 854–6
[54] Bratescu M A, Cho S P, Takai O and Saito N 2011 *J. Phys. Chem.* C **115** 24569–76
[55] Chen Q, Kaneko T and Hatakeyama R 2011 *30th Int. Conf. on Phenomena in Ionized Gases*
[56] Mariotti D, Švrček V, Hamilton J W J, Schmidt M and Kondo M 2012 *Adv. Funct. Mater.* **22** 954–64
[57] Locke B R and Shih K Y 2011 *Plasma Sources Sci. Technol.* **20** 034006
[58] Lukeš P 2001 Water treatment by pulsed streamer corona discharge *PhD Thesis* Institute of Plasma Physics